

# Measuring the time a tunnelling atom spends in the barrier

Ramón Ramos<sup>1</sup>, David Spierings<sup>1</sup>, Isabelle Racicot<sup>1</sup> & Aephraim M. Steinberg<sup>1,2</sup>

<sup>1</sup>Centre for Quantum Information and Quantum Control and Institute for Optical Sciences, Department of Physics, University of Toronto, 60 St. George Street, Toronto, Ontario M5S 1A7, Canada.

<sup>2</sup>Canadian Institute For Advanced Research, MaRS Centre, West Tower 661 University Ave., Toronto, Ontario M5G 1M1, Canada.

**Tunnelling is one of the most paradigmatic and evocative phenomena of quantum physics, underlying processes such as photosynthesis and nuclear fusion, as well as devices ranging from SQUID magnetometers to superconducting qubits for quantum computers. The question of how *long* a particle takes to tunnel, however, has remained controversial since the first attempts to calculate it<sup>1,2</sup>, which relied on the group delay. It is now well understood that this delay (the arrival time of the transmitted wave packet peak at the far side of the barrier) can be smaller than the barrier thickness divided by the speed of light, without violating causality. There have been a number of experiments confirming this<sup>3-6</sup>, and even a recent one claiming that tunnelling may take no time at all<sup>7</sup>. There have also been efforts to identify another timescale, which would better describe how long a given particle *spends* in the barrier region<sup>8-10</sup>. Here we present a direct measurement of such a time, studying Bose-condensed <sup>87</sup>Rb atoms tunnelling through a 1.3- $\mu$ m thick optical barrier. By localizing**

**a pseudo-magnetic field inside the barrier, we use the spin precession of the atoms as a clock to measure the time it takes them to cross the classically forbidden region. We find a traversal time of 0.62(7) ms and study its dependence on incident energy. In addition to finally shedding light on the fundamental question of the tunnelling time, this experiment lays the groundwork for addressing deep foundational questions about history in quantum mechanics: for instance, what can we learn about where a particle was at earlier times by observing where it is now<sup>11-13</sup>?**

While the earliest attempts to calculate the time a tunnelling particle spends in the barrier region\* addressed the propagation delay for a wave packet peak, work in the 1980s, particularly by Büttiker and Landauer<sup>14,15</sup>, shifted the discussion to an ‘interaction time’, the time actually spent by a particle in the barrier. This was motivated by the prediction<sup>16</sup> that in certain regimes, the wave packet delay (sometimes referred to as the ‘phase time’ or ‘Wigner time’<sup>2</sup>) could appear to be superluminal, suggesting that it does not reflect the duration of the tunnelling event. Büttiker and Landauer provided arguments in favour of a ‘semiclassical time’ equal to  $md/\hbar\kappa$ , where  $m$  is the mass,  $d$  is the barrier thickness, and  $\kappa = \sqrt{2m(V_0 - E)}/\hbar$  is the evanescent decay constant in the tunnelling regime ( $E$  is the incident energy and  $V_0$  is the barrier height); it should be noted that unlike the group delay, this grows linearly with  $d$  and is thus generally not superluminal. As we shall discuss in depth below, another way of defining the tunnelling duration is via the effect a particle has on an auxiliary ‘clock’ degree of freedom.

A number of experiments have sought to measure tunnelling times. Several optical experiments<sup>3-6</sup>

---

\*not to be confused with the lifetime of a quasi-bound state

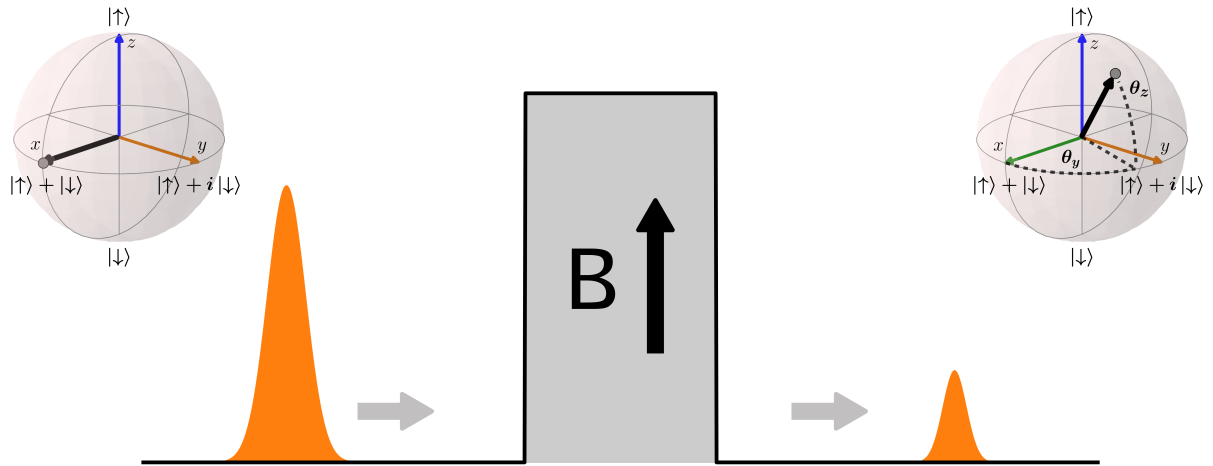


Figure 1: Larmor clock. A weak magnetic field  $B$  pointing in the  $z$ -direction is localized inside the potential barrier. A particle with spin-1/2 pointing initially along the  $x$ -direction impinges on the barrier, and after transmission, the spin has precessed in the  $xy$  plane with a Larmor frequency  $\omega_L$  and tilted towards the  $z$ -axis, as depicted in the Bloch sphere. The  $|\uparrow\rangle$  and  $|\downarrow\rangle$  states are the eigenstates of the system in the presence of the magnetic field along the  $z$ -axis. The Larmor times are then defined as  $\tau_y = \theta_y/\omega_L$  and  $\tau_z = \theta_z/\omega_L$ .

have confirmed the superluminal nature of the group delay, and some have attempted to probe other timescales<sup>17,18</sup>. A pioneering experiment studying quantum tunnelling in a Josephson junction<sup>19</sup> was the first attempt to apply the insights of Büttiker and Landauer to instead probe the duration of the tunnelling event itself and offered qualitative agreement with the ‘semiclassical time’.

Recently, there has been an explosion of experimental interest in the area due to the Keller group’s development of the ‘attoclock’<sup>20</sup>. These experiments<sup>7,21–25</sup> use strong-field ionisation in a circularly polarized field to determine how much time elapses between the ionising field reaching its maximum and an electron finally escaping. Intuitively, one might therefore expect such times to be described by the group delay, although there have been multiple theoretical approaches and no small amount of controversy. In this setup, rather than impinging upon a barrier, the electron escapes from a quasi-bound state<sup>†</sup>. Therefore, it is impossible to identify a time at which the event ‘starts’, as opposed to merely the moment at which the field reaches its maximum. The problem is further complicated by atomic-physics effects which generate additional delays unrelated to the tunnelling event. The most recent experiment, attempting to properly account for these, made the dramatic claim that tunnelling is essentially instantaneous<sup>7</sup>. There has also been an experiment probing the time delay between two tunnel-coupled momentum components of atoms oscillating in the wells of an optical lattice<sup>27</sup>, although it was unable to discriminate between the different theories.

To provide an operational definition of the tunnelling time, it is natural to devise a ‘clock’

---

<sup>†</sup>see the distinction made early on by Landauer<sup>26</sup>

which ticks only while the particle is present in the barrier region. The Larmor clock, originally introduced by Baz'28 and Rybachenko29, is the most famous example of such a thought experiment. If an ensemble of polarized spin-1/2 particles impinges on a barrier, localizing a magnetic field on the barrier region alone will cause the spins to precess only while the particles are under the barrier (see Fig. 1). Considering incident particles polarized in the  $x$ -direction and a magnetic field along  $z$ , one would expect the spin to precess by an angle  $\theta = \omega_L \tau$ , where  $\omega_L$  is the Larmor frequency and  $\tau$  is the time spent in the barrier. By working in the limit of a weak magnetic field ( $\omega_L \rightarrow 0$ ), this time can be measured without significantly perturbing the tunnelling particle. Büttiker15 noted that even in this limit, measurement back-action cannot be neglected, and results in preferential transmission of atoms aligned with the magnetic field. This leads to two spin rotation angles: a precession in the plane orthogonal to the applied magnetic field,  $\theta_y$ , as well as an alignment along the direction of the field,  $\theta_z$ . He defined times associated with the spin projections:  $\tau_z$ ,  $\tau_y$  and  $\tau_x = \sqrt{\tau_y^2 + \tau_z^2}$ , the latter often known as the 'Büttiker time'. It turns out that combinations of two such quantities appear in other theoretical treatments as a single complex number30,31, but researchers were hesitant to accept complex-valued times without a clear interpretation. Later, Steinberg11,12 associated  $\tau_y$  and  $\tau_z$  with the real and imaginary parts of the 'weak value'13 of a dwell-time operator, thereby providing them with distinct interpretations as the inherent tunnelling time and the measurement back-action, respectively.

We have built an experiment to implement the Larmor clock, making use of the long de Broglie wavelengths achievable in atomic Bose-Einstein condensates and the remarkable degree of control possible in such systems, both for tailoring optical potentials and for manipulating and

measuring spins. The spatial resolution of the potentials is limited only by the wavelength of the laser light used, and at our energy scales – which are on the order of  $E/k_b \sim 1$  nK (10's of feV) – the tunnelling probability is sizable, while the millisecond-level timescales are convenient to probe experimentally. A two-photon Raman transition driven by the barrier beam itself couples the states of a pseudo spin-1/2 system, generating our Larmor clock: the effective Larmor frequency  $\omega_L$  is set by the two-photon Rabi frequency  $\Omega$  of the Raman transition. Using this scheme, we are able to determine the barrier traversal time in our system by measuring the final spin state of the transmitted atoms.

We prepare a degenerate gas of approximately 8000  $^{87}\text{Rb}$  atoms in the  $5S_{1/2} |F = 2, m_F = 2\rangle$  state ( $F$  and  $m_F$  denote the hyperfine and Zeeman quantum numbers respectively) in a crossed dipole trap. One of the trap beams is turned off and the atoms are left free to move longitudinally in a quasi one-dimensional waveguide. We decrease the effective temperature of the atoms using matter-wave lensing (see Methods), resulting in an rms velocity spread of 0.45(15) mm/s, or an equivalent effective temperature of 2(1) nK ( $\lambda_{\text{dB}} = 4(1) \mu\text{m}$ ). We then push the atoms towards a 1.3  $\mu\text{m}$  Gaussian barrier, formed by a focused blue-detuned beam (see Methods), using a variable-duration magnetic gradient pulse to set the velocity. We have previously observed tunnelling through this potential in two different contexts: escape from a quasi-bound state<sup>32,33</sup>; and in a single-collision geometry<sup>34</sup>, such as the one studied here. While the atoms approach the potential barrier, rapid adiabatic passage is used to transfer the atoms from their initial spin state to the  $|2, 0\rangle$  state. An effective spin-1/2 is encoded in the  $|2, 0\rangle$  and  $|1, 0\rangle$  hyperfine clock states denoted by  $|+x\rangle = \frac{|\uparrow\rangle + |\downarrow\rangle}{\sqrt{2}}$  and  $|-x\rangle = \frac{|\uparrow\rangle - |\downarrow\rangle}{\sqrt{2}}$  respectively (Fig. 2). The barrier light is phase-modulated at

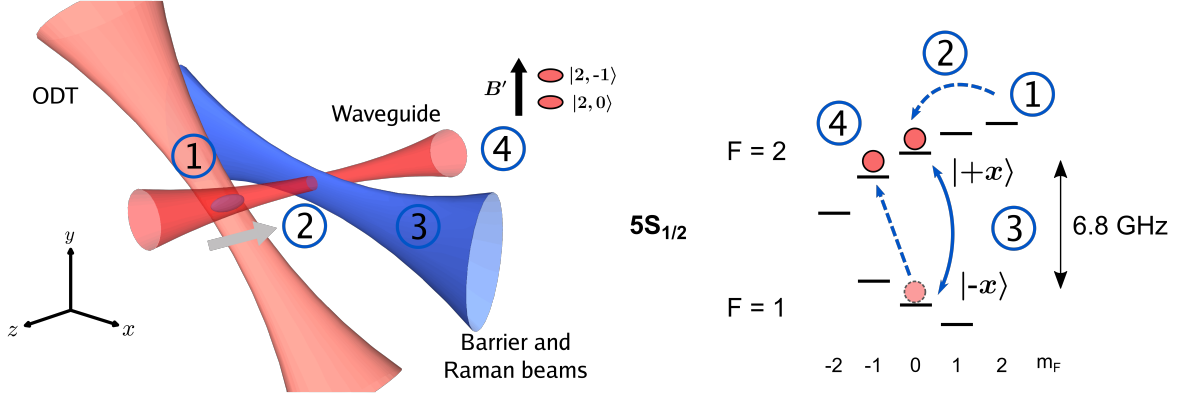


Figure 2: Experimental setup and sequence. We create a Bose-Einstein condensate in the  $|F = 2, m_F = 2\rangle$  state in a crossed dipole trap formed by an optical waveguide and a perpendicular beam (ODT) intersecting it. (1) After the effective temperature of the cloud is lowered, the atoms are pushed, by a pulsed magnetic field gradient, along the waveguide in the  $-z$  direction towards a blue-detuned beam which generates the potential barrier and the pair of Raman beams. (2) While the atoms travel towards the barrier we use rapid adiabatic passage to transfer them to the  $|2, 0\rangle$  ( $|+x\rangle$ ) state. (3) During the interaction with the barrier, the pair of Raman beams couples the  $|+x\rangle$  and  $| -x \rangle$  states. (4) To perform the read-out sequence, the atoms which were coupled to  $| -x \rangle$  are transferred to the  $|2, -1\rangle$  state, after which we perform a Stern-Gerlach measurement to separately image both of the states.

the 6.8-GHz hyperfine frequency, thus creating a pair of Raman beams that couple the  $|+x\rangle$  and  $| -x\rangle$  states. In the interaction picture, the pseudo-magnetic field generated by the Raman beams points along the  $z$ -direction of the Bloch sphere. After the collision with the barrier is complete, we perform a final rapid adiabatic passage sweep from  $| -x\rangle$  to  $|2, -1\rangle$ . A subsequent Stern-Gerlach sequence separates the two spin states, allowing us to determine the populations of  $|\pm x\rangle$ .

We begin by testing the implementation of the Larmor clock in free space. For this purpose, we remove the potential barrier but keep the pseudo-magnetic field on by changing the barrier wavelength to a nearby tune-out wavelength (see Fig. 3 and Methods for details). The precession angle tells us how much time the atoms spend in the region with the localized pseudo-magnetic field. The results without the barrier (see Fig. 3 b) show an expected  $1/v$  dependence, where  $v$  is the velocity of the atoms. With our knowledge of the barrier width, we can extract the Rabi frequency of the two-photon transition.

After verifying the behaviour of the clock, we move to the case of a repulsive barrier. In this case, after the interaction with the barrier and the Raman beams, each atom will be either transmitted or reflected, with its spin in a superposition of the  $|+x\rangle$  and  $| -x\rangle$  states (see Fig. 4a). At high energies, the barrier has little effect on the atoms and the precession angle scales inversely with velocity as before. From these points, we deduce the Rabi frequency. We perform the tunnelling measurement with a 135(8) nK barrier height, corresponding to 5.1 mm/s, and a Rabi frequency of  $\Omega = 2\pi \times 220(40)$  Hz.

We investigate the two Larmor times by performing full spin-tomography of the transmitted

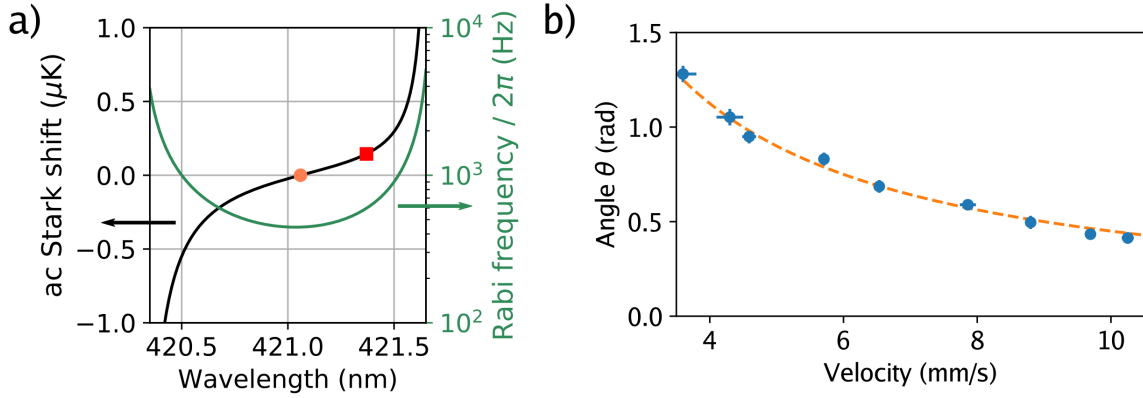


Figure 3: Larmor clock implementation. **a**, Scalar ac Stark shift (black line) created by the tunable laser beam used for the optical potential. The two points represent the wavelengths used in the experiment: the orange dot is at the wavelength for which the barrier height vanishes (tune-out wavelength) and where the free-space Larmor measurement is performed, and the red square is at the wavelength used to create a 135 nK potential barrier. The pair of Raman beams, with two-photon Rabi frequency indicated by the green line, is created with the same beam as the barrier. **b**, Measurement of the precession angle at the tune-out wavelength. The dashed line is a one parameter fit to the expression  $\Omega d/v$ , where  $d$  is the effective barrier width,  $v$  is the incident velocity of the atoms and  $\Omega$  is the Rabi frequency, left as a free parameter. We find a Rabi frequency of  $\Omega = 2\pi \times 440(10)$  Hz. The Rabi frequency  $\Omega$  can be controlled independently of the barrier height and was reduced for the tunnelling data (see Methods).

spin-1/2 particles. Rotations after the scattering event allow us to measure the spin components along the  $x$ ,  $y$ , and  $z$ -axes of the Bloch sphere (see Fig. 4b). From the different projections, we find the traversal time  $\tau_y$  and the time  $\tau_z$  associated with the back-action of the measurement (see Fig. 4c). At the lowest incident velocity (4.1 mm/s), we observe a transmission probability of 3%. Given the energy-dependence of the transmission, we calculate that the transmitted atoms have a velocity distribution with a peak at 4.8 mm/s, corresponding to  $\kappa d \simeq 3$ . About 3/4 of this distribution corresponds to energies below the barrier height. The measured traversal time  $\tau_y$  is 0.62(7) ms.

The experimental data are in good agreement with one-dimensional two-component time-dependent Schrödinger simulations with no free parameters (see Fig. 4c), while Gross-Pitaevskii simulations show no significant modifications due to the presence of interactions. Furthermore, the theoretical prediction given by the weak value formalism describes our results well (see Methods). In contrast, the ‘semiclassical time’ disagrees with  $\tau_x$  by more than three standard deviations for the lowest velocities.

This is, to our knowledge, the first direct measurement of the time massive particles spend in a barrier region, implementing the Larmor-time thought experiment of Baz’, Rybachenko and Büttiker. For a range of incident velocities, we can observe both the time spent in the barrier and the spin-rotation due to measurement back-action, clearly separating the two effects. We see that as one heads deeper into the quantum regime, the back-action grows in importance, and our results are consistent with the prediction that the tunnelling time begins to decrease<sup>15</sup>. Our results are in-

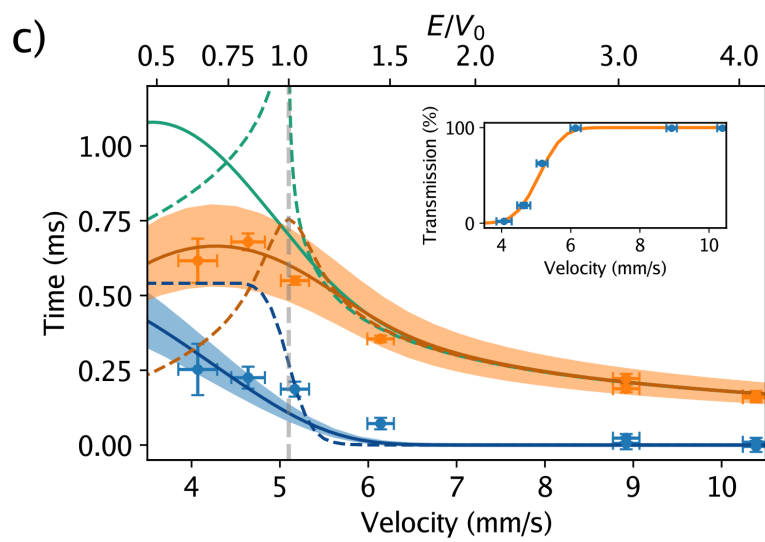
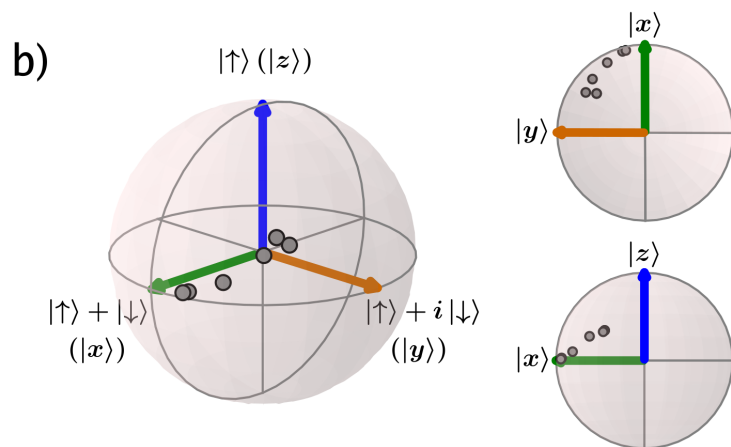
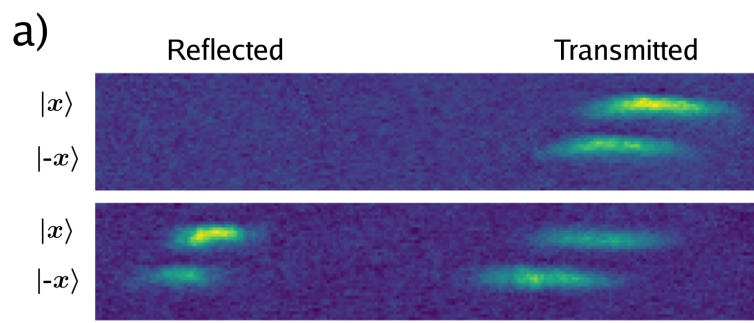


Figure 4: Traversal time of an atomic wavepacket through an optical potential. **a**, Absorption images of the atomic densities after the interaction with a 135 nK barrier and the Raman beams for incident energies of 400 nK (top) and 140 nK (bottom). The precession angles for the transmitted atoms are obtained by doing full tomography on the spin-1/2 system. **b**, Obtained spin projections for the different incident velocities. The top right and bottom right figures show cuts along the  $xy$  and  $xz$  planes. **c**, Experimental data of the Larmor times  $\tau_y$  (orange dots) and  $\tau_z$  (blue dots) as a function of incident velocity. The dashed gray line corresponds to the velocity matching the height of the barrier (5.1 mm/s). Light orange and blue regions are 1D two-component time-dependent Schrödinger simulations, and the bands represent the uncertainty on the measured Rabi frequency. The dashed lines are monochromatic theory predictions for the Larmor times  $\tau_y$  (orange) and  $\tau_z$  (blue), and the semiclassical time (green). The corresponding solid lines are calculated by taking into account the 0.45 mm/s velocity spread of the initial wavepacket. **Inset**, Transmission probability data (blue dots) and two-component time-dependent Schrödinger simulations using a 0.45 mm/s velocity spread wavepacket (orange line).

consistent with claims that tunnelling takes ‘zero time’<sup>7,20</sup>. Beyond resolving the controversy over how long a tunnelling particle spends in the barrier region, the experimental approach pioneered here opens a new window on quantum measurement and the broad question of how much one can infer about the history of a quantum particle. In particular, it will enable measurements of *where* within a barrier transmitted and reflected particles each spend their time<sup>11,12</sup>. As it is predicted that these exhibit nonclassical behaviour, their study as the system is made ‘more classical’ by the introduction of dissipation or atomic interactions promises to offer a new perspective on the quantum-classical boundary.

## Methods

**Experimental setup.** We Bose-condense  $8 \times 10^3$  <sup>87</sup>Rb atoms in a 1064 nm crossed dipole trap. The trap is composed of two beams: an elongated beam which we refer to as the atom waveguide (with a waist of 15  $\mu\text{m}$  and a Rayleigh range of  $z_0 \approx 600$   $\mu\text{m}$ ) and an orthogonal beam intersecting the waveguide nearly 150  $\mu\text{m}$  away from its centre. The atoms start at the intersection of the two beams. The atom waveguide has radial and longitudinal frequencies of  $\nu_r = 220$  Hz and  $\nu_l = 2.7$  Hz. The barrier beam, formed by a 421 nm laser focused to 1.3  $\mu\text{m}$  (see below), intersects the waveguide close to its centre. The longitudinal trap frequency sets the minimum velocity at which the atoms meet the barrier, since the waveguide curvature produces an acceleration of  $5 \times 10^{-2}$   $\text{m/s}^2$ .

**Matter-wave lensing.** We use delta kick cooling<sup>35–39</sup>, also referred to as matter-wave lensing, to decrease the effective temperature of the atoms from 15 nK to 2(1) nK, or a corresponding rms velocity spread of 0.45(15) mm/s. At this temperature, the atoms have a thermal de Broglie wavelength of  $\lambda_{dB} = 4(1) \mu\text{m}$ . The cooling procedure is as follows: the atoms start in a crossed dipole trap, they are released from one of these beams (ODT) and expand in the atom waveguide for 9 ms (to approximately four times the initial cloud size), and then a quasi-harmonic trap with a frequency of  $\omega = 2\pi \times 50(5) \text{ Hz}$  created by the ODT beam is flashed for 1.1 ms to collimate the atomic wavepacket. The amount of expansion is limited by the radius of the beam ( $1/e^2$  radius of 100  $\mu\text{m}$ ): this expansion time is kept short enough that the atoms remain within the harmonic region of the Gaussian potential. The condensate has a final longitudinal rms radius of 15  $\mu\text{m}$ . We have achieved temperatures as low as 0.9 nK using this technique by reducing the initial atom number, but in order to work at higher atom numbers, we perform this experiment at 2 nK.

**Potential barrier and Raman beams.** The light for the barrier and the Raman beams is created by a homemade 421 nm external cavity diode laser (ECDL) in Littrow configuration. We set the frequency of this beam in the vicinity of one of the rubidium tune-out wavelengths (421.07 nm) located between the  $5S_{1/2} \rightarrow 6P_{1/2}$  (421.7 nm) and the  $5S_{1/2} \rightarrow 6P_{3/2}$  (420.3 nm) transitions. To generate the pair of Raman beams, the beam passes through a 6.8 GHz electro-optic phase modulator using a modulation depth of  $\beta \simeq 0.3$  which creates a pair of sidebands in the optical spectrum. About 5% of the optical power goes to the sidebands. The generated sidebands have opposite phases and act destructively when used along with the carrier to drive Raman transitions. An etalon with a FWHM bandwidth of 12 GHz is therefore used to remove one of the sidebands.

We can control the Rabi frequency without modifying the power of the Raman beams, by adjusting the modulation depth  $\beta$ . This is monitored by detecting the beat signal between the carrier and the remaining sideband on a fast photodiode.

The barrier light is sent to the science chamber, where it is focused to a  $1/e^2$  radius of  $w_z = 1.3 \mu\text{m}$  along the  $z$ -direction, while along the  $y$ -direction it is scanned with an acousto-optical deflector to create a flat,  $50 \mu\text{m}$  wide, time-averaged potential. The Rayleigh range of the beam is  $8 \mu\text{m}$ , larger than the transverse radius of the condensate ( $\sim 2.5 \mu\text{m}$ ). We can set the wavelength to  $421.38 \text{ nm}$ , where a power of approximately  $0.5 \text{ mW}$  generates a repulsive potential as large as  $V_0/k_b \sim 180 \text{ nK}$  (given by the scalar ac Stark shift, as the vector light shift vanishes for the clock states). A magnetic field pointing along the propagation axis of the beams ( $x$ -direction) sets the quantization axis. The beams are circularly polarized, to drive  $\sigma^+ - \sigma^+$  Raman transitions.

To calibrate the Rabi frequency, we study high-velocity incident atoms traversing the barrier, which to a good approximation undergo free propagation. The spin rotation due to the Raman beams is given by  $\theta = \int dt \Omega_0 e^{-2(vt)^2/w_z^2} = \Omega_0 d/v$ , where  $v$  is the velocity of the atoms and  $d = \sqrt{\pi/2} w_z$  is the effective barrier width. The Rabi frequency can also be calibrated at the tune-out wavelength. Accounting for the difference in ac Stark shift between the barrier and tune-out wavelengths, and frequency-dependent transmission due to etaloning effects in our chamber windows, the two techniques are in good agreement. However, due to the limited tunability of the barrier ECDL, we utilize the first method to calibrate the Rabi frequency.

**Larmor time calculations.** We calculate the characteristic Larmor times using the weak measurement formalism<sup>13</sup>. The projection operator onto the barrier region,  $\Theta$ , has eigenvalues 1 (for particles in the barrier region) and 0 (for particles outside). A dwell time operator  $D \equiv \int_{-\infty}^{\infty} dt \Theta(t)$  provides a measure of time spent in the barrier. However, its expectation value includes contributions from both transmitted and reflected atoms. Steinberg<sup>11,12</sup> showed that the weak value of this operator,  $D_w = \tau_y + i\tau_z = \langle f|D|i\rangle/\langle f|i\rangle$  where  $i$  refers to the initial state and  $f$  to the final state, can be understood as the conditional dwell time of a particle which is prepared in the  $|i\rangle$  state and postselected in the  $|f\rangle$  state. In our experiment, the initial state corresponds to atoms incident on the barrier from the left, while the final state corresponds to transmitted atoms on the right side of the barrier. As originally shown by Büttiker<sup>15</sup>, these Larmor times can also be calculated as follows:  $\tau_y = -\hbar\partial\phi/\partial V$  and  $\tau_z = -\hbar\partial|T|/\partial V$ , where  $\phi$  and  $|T|$  are the phase and the magnitude of the transmission amplitude, respectively.

Using the transfer matrix method, we solve for the conditional dwell times at different incident energies numerically. In the experiment, the Larmor probe is implemented by the pair of Raman beams; therefore, in the calculations, we obtain the dwell times by integrating over the Gaussian region of the barrier (the top-hat function  $\Theta$  is replaced with a Gaussian weight function, representing the local strength of the interaction with the clock). This integration region extends beyond the turning points of the barrier for the range of incident energies, and we calculate that about 40% of the measured time for the lowest incident energy comes from the time spent in the classically forbidden region.

**Spin preparation, rotation and readout.** After we accelerate the atoms using a 15 G/cm magnetic gradient pulse for a variable time (0 - 0.9 ms), we prepare the spin state of the atoms. While the atoms travel towards the barrier, we ramp up the magnetic field to approximately 40 G. The high magnetic field causes a difference in successive energy splittings of the  $F = 2$  manifold of 210 kHz thanks to the quadratic Zeeman shift. This allows us to transfer the atoms from  $|2, 2\rangle$  (in which they Bose-condensed) to  $|2, 0\rangle$  using a 1 ms radio-frequency rapid adiabatic passage. A multi-loop antenna provides the rf coupling with a Rabi frequency of approximately  $\Omega_{\text{rf}} \approx 2\pi \times 9$  kHz. The transfer efficiency is greater than 95%, and the atoms left behind can be identified and do not affect the subsequent dynamics in the experiment. The total preparation sequence lasts for 9 ms. Since the clock transition has a field dependence of 575 Hz/G<sup>2</sup>, we lower the magnetic field to 1 G prior to the interaction with the Raman beams to reduce our sensitivity to magnetic noise.

For the read-out sequence, we again increase the magnetic field to 40 G. Due to the quadratic Zeeman shift, the frequency difference between the  $|1, 0\rangle$  to  $|2, -1\rangle$  and the  $|1, -1\rangle$  to  $|2, 0\rangle$  transitions is 110 kHz. We transfer the atoms through a rapid adiabatic passage from  $|1, 0\rangle$  to  $|2, -1\rangle$  in 1.5 ms. The transfer efficiency is 90%. This sequence lasts for 8.5 ms. Subsequently, we lower the magnetic field to 1 G and perform a 5.5 ms time-of-flight with a 40 G/cm magnetic gradient to implement a Stern-Gerlach measurement and simultaneously image both of the final states.

We can only directly measure the hyperfine states  $|+x\rangle$  ( $|2, 0\rangle$ ) and  $|-x\rangle$  ( $|1, 0\rangle$ ), thus obtaining  $\langle Sx \rangle$ . To complete the tomography, after the interaction with the barrier we apply a microwave pulse addressing the  $|+x\rangle$  and the  $|-x\rangle$  states to perform a  $\pi/2$  rotation along the  $z$ -axis to measure

$\langle Sy \rangle$ . Similarly, we rotate the spin by a  $\pi/2$  angle along the  $y$ -axis, through a phase shift of  $\pi/2$  radians in the driving field, to measure  $\langle Sz \rangle$ . The rotations are done with a dipole antenna driving the atoms with a Rabi frequency of  $\Omega_{\text{mw}} = 2\pi \times 2.4$  kHz. To identify and account for possible systematic errors such as imperfect  $\pi/2$  rotations or population transfer in the read-out sequence, we also measure the  $-x$ ,  $-y$  and  $-z$  projections. We periodically calibrate the phase between the microwave source and the Raman beams since drifts in the ECDL frequency and changes in the etalon due to temperature fluctuations can occur. The phase calibration is performed as follows: a spin rotation along the  $z$ -axis, for atoms with an incident velocity well above the barrier height, is induced by the Raman beams and it is followed by a microwave pulse tuned to provide a  $\pi/2$  rotation about a torque vector which lies in the  $yz$  plane of the Bloch sphere, its angle on this plane depending on the microwave source phase (relative to that of the Raman beams). We repeat the procedure while scanning the phase of the microwave source and determine the phase difference from the sinusoidal behaviour of the measured hyperfine populations. For this calibration, we use a 120(7) nK barrier and an incident velocity of 8.70(15) mm/s. The typical phase drift between calibrations is 90 mrad and has been included in the measurement uncertainties.

## References

1. MacColl, L. A. Note on the transmission and reflection of wave packets by potential barriers. *Phys. Rev.* **40**, 621 (1932).
2. Wigner, E. P. Lower limit for the energy derivative of the scattering phase shift. *Phys. Rev.* **98**, 145 (1955).

3. Ranfagni, A., Mugnai, D., Fabeni, P. & Pazzi, G. P. Delay-time measurements in narrowed waveguides as a test of tunneling. *Appl. Phys. Lett.* **58**, 774 (1991).
4. Enders, A. & Nimtz, G. On superluminal barrier traversal. *J. Phys. I* **2**, 1693 (1992).
5. Steinberg, A. M., Kwiat, P. G. & Chiao, R. Y. Measurement of the single-photon tunneling time. *Phys. Rev. Lett.* **71**, 708 (1993).
6. Spielmann, C., Szepöcs, R., Stingl, A. & Krausz, F. Tunneling of optical pulses through photonic band gaps. *Phys. Rev. Lett.* **73**, 2308 (1994).
7. Sainadh, U. S. *et al.* Attosecond angular streaking and tunnelling time in atomic hydrogen. *Nature* **568**, 75 (2019).
8. Hauge, E. H. & Støvneng, J. A. Tunneling times: A critical review. *Rev. Mod. Phys.* **61**, 917 (1989).
9. Landauer, R. & Martin, T. Barrier interaction time in tunneling. *Rev. Mod. Phys.* **66**, 217 (1994).
10. Chiao, R. Y. & Steinberg, A. M. Tunneling times and superluminality. In *Prog. Opt.* **XXXVII**, 345 (1997).
11. Steinberg, A. M. How much time does a tunneling particle spend in the barrier region? *Phys. Rev. Lett.* **74**, 2405 (1995).
12. Steinberg, A. M. Conditional probabilities in quantum theory and the tunneling-time controversy. *Phys. Rev. A* **52**, 32 (1995).

13. Y. Aharonov, D. Z. Albert, & Vaidman, L. How the result of a measurement of a component of the spin of a spin-1/2 particle can turn out to be 100. *Phys. Rev. Lett.* **60**, 2325 (1988).
14. Büttiker, M. & Landauer, R. Traversal time for tunneling. *Phys. Rev. Lett.* **49**, 1739 (1982).
15. Büttiker, M. Larmor precession and the traversal time for tunneling. *Phys. Rev. B* **27**, 6178 (1983).
16. Hartman, T. E. Tunneling of a wave packet. *J. Appl. Phys.* **33**, 3427 (1962).
17. Deutsch, M. & Golub, J. Optical Larmor clock: Measurement of the photonic tunneling time. *Phys. Rev. A* **53**, 434 (1996).
18. Balcou, P. & Dutriaux, L. Dual Optical Tunneling Times in Frustrated Total Internal Reflection. *Phys. Rev. Lett.* **78**, 851 (1997).
19. Esteve, D. *et al.* Observation of the Temporal Decoupling Effect on the Macroscopic Quantum Tunneling of a Josephson Junction. *Phys. Scr.* **29**, 121 (1989).
20. Eckle, P. *et al.* Attosecond angular streaking. *Nat. Phys.* **4**, 565 (2008).
21. Eckle, P. *et al.* Attosecond ionization and tunneling delay time measurements in helium. *Science* **322**, 1525 (2008).
22. Pfeiffer, A. N., Cirelli, C., Smolarski, M. & Keller, U. Recent attoclock measurements of strong field ionization. *Chem. Phys.* **414**, 84 (2013).
23. Landsman, A. S. *et al.* Ultrafast resolution of tunneling delay time. *Optica* **1**, 343 (2014).

24. Zimmermann, T., Mishra, S., Doran, B. R., Gordon, D. F. & Landsman, A. S. Tunneling Time and Weak Measurement in Strong Field Ionization. *Phys. Rev. Lett.* **116**, 233603 (2016).
25. Camus, N. *et al.* Experimental Evidence for Quantum Tunneling Time. *Phys. Rev. Lett.* **119**, 023201 (2017).
26. Landauer, R. Barrier traversal time. *Nature* **341**, 567 (1989).
27. Fortun, A. *et al.* Direct Tunneling Delay Time Measurement in an Optical Lattice. *Phys. Rev. Lett.* **117**, 010401 (2016).
28. Baz', A. Lifetime of Intermediate States. *Sov. J. Nucl. Phys.* **4**, 182 (1966).
29. Rybachenko, V. Time of Penetration of a Particle through a Potential Barrier. *Sov. J. Nucl. Phys.* **5**, 635 (1967).
30. Pollak, E. & Miller, W. H. New physical interpretation for time in scattering theory. *Phys. Rev. Lett.* **53**, 115 (1984).
31. Sokolovski, D. & Baskin, L. M. Traversal time in quantum scattering. *Phys. Rev. A* **36**, 4604 (1987).
32. Potnis, S., Ramos, R., Maeda, K., Carr, L. D. & Steinberg, A. M. Interaction-Assisted Quantum Tunneling of a Bose-Einstein Condensate out of a Single Trapping Well. *Phys. Rev. Lett.* **118**, 060402 (2017).
33. Zhao, X. *et al.* Macroscopic quantum tunneling escape of Bose-Einstein condensates. *Phys. Rev. A* **96**, 63601 (2017).

34. Ramos, R., Spierings, D., Potnis, S. & Steinberg, A. M. Atom-optics knife edge: Measuring narrow momentum distributions. *Phys. Rev. A* **98**, 23611 (2018).
35. Chu, S., Bjorkholm, J. E., Ashkin, A., Gordon, J. P. & Hollberg, L. W. Proposal for optically cooling atoms to temperatures of the order of  $10^{-6}$  K. *Opt. Lett.* **11**, 73 (1986).
36. Ammann, H. & Christensen, N. Delta Kick Cooling: A New Method for Cooling Atoms. *Phys. Rev. Lett.* **78**, 2088 (1997).
37. Morinaga, M., Bouchoule, I., Karam, J.-C. & Salomon, C. Manipulation of Motional Quantum States of Neutral Atoms. *Phys. Rev. Lett.* **83**, 4037 (1999).
38. Maréchal, E. *et al.* Longitudinal focusing of an atomic cloud using pulsed magnetic forces. *Phys. Rev. A* **59**, 4636 (1999).
39. Myrskog, S. H., Fox, J. K., Moon, H. S., Kim, J. B. & Steinberg, A. M. Modified "delta -kick cooling" using magnetic field gradients. *Phys. Rev. A* **61**, 053412 (2000).

**Acknowledgements** We wish to acknowledge years of hard work by the students, postdocs, and technologists who created this Bose-Einstein condensation apparatus and helped turn it into the robust, precise machine which made the present experiment possible: Ana Jofre, Mirco Siercke, Chris Ellenor, Marcelo Martinelli, Rockson Chang, Shreyas Potnis, and Alan Stummer. We thank Joseph Thywissen, Amar Vutha, Joseph McGowan, Kent Bonsma-Fisher and Aharon Brodutch for valuable discussions. This work was supported by NSERC and the Fetzer Franklin Fund of the John E. Fetzer Memorial Trust. A.M.S. is a fellow of CIFAR. R.R. acknowledges support from CONACYT.

**Author contributions** R.R., D.S. and I.R. performed the experiments. A.M.S. supervised the work.

All authors made contributions to the work, discussed the results and contributed to the writing of the manuscript.

**Competing Interests** The authors declare no competing financial interests.